JME

Journal of Mining & Environment,
Vol. 9, No. 4, 2018, 817-828.
DOI: 10.22044/jme.2018.6604.1482

A new 2D block ordering system for wavelet-based multi-resolution up-scaling

B. Tokhmechi[1*], M. Rabiei[2], H. Azizi[2] and V. Rasouli[2]

1. Faculty of Mining, Petroleum & Geophysics Engineering, Shahrood University of Technology, Shahrood, Iran
2. Department of Petroleum Engineering, University of North Dakota, Grand Forks, USA

Received 6 January 2018; received in revised form 11 May 2018; accepted 12 May 2018
**Corresponding author: tokhmechi@ut.ac.ir (B. Tokhmechi).*

Abstract
A complete and accurate analysis of the complex spatial structure of heterogeneous hydrocarbon reservoirs requires detailed geological models, i.e. fine resolution models. Due to the high computational cost of simulating such models, single resolution up-scaling techniques are commonly used to reduce the volume of the simulated models at the expense of losing the precision. Several multi-scale techniques have also been developed for simulating heterogeneous reservoirs including those in which a limited number of blocks down-scale, i.e. splitting coarse blocks into fine cells around the well-zones in the case of simulation of hydraulic fracturing. In these cases, locally computed basis functions are employed to construct a global solver at a coarse-scale such as wavelet- and kernel-based up-scaling techniques. In this paper, a novel/robust 2D block-ordering system is presented, which enables solving multi-resolution up-scaling fluid flow simulations. The results will be described for a simple model, and fluid flow equations will be developed in order to show the structure of transmissibility matrix. It is confirmed that with a developed block-ordering system not only the accuracy of history match increases but also the CPU time decreases.

Keywords: *Kernel, History Matching, Multi-resolution Up-scaling, CPU Time.*

1. Introduction

In simulating the fluid flow in porous media, a linear system of equations is solved by relating a vector of unknown variables to a vector of known values via a square coefficient matrix. The computer time and storage requirements of a simulation run can be reduced by changing the structure of the coefficient matrix using different grid block-ordering schemes.

Natural ordering by rows (Figure 1a), by columns (Figure 1b), D-4 ordering (Figure 1c), cyclic-2 ordering (Figure 1d), and D-2 ordering schemes (Figure 1e) are examples of block-ordering methods commonly used in single scale grid blocks [1, 2]. For example, Figure 1a, block number 1, has intersection with blocks 2 and 7 (which are shaded in the first row and first column of the right hand side shaded matrix), and block number 2 has intersection with blocks 1, 3, and 8 (which are shaded in the second row and second column of the right hand side shaded matrix). The coefficient matrices corresponding to these ordering schemes can be formulated as a banded matrix (tridiagonal, pentadiagonal, or heptadiagonal non-zero entries) depending on the dimension of the problem. These banded matrices are composed of many zero entries outside the band envelop between the uppermost and lowermost diagonals, which are excluded from the operations.

In these banded structures, the bandwidth is defined as the maximum number of elements within the band envelop in any row of the matrix [3]. Bandwidth is expressed as $2 \times n_i + 1$, in which n_i is the number of blocks in the direction we consider for ordering. For example, in Figures 1a ($n_x = 6$) and 1b ($n_y = 4$), bandwidth is equal to 13 and 9, respectively. Since all computations are performed on the matrix entries within the

bands, problems with smaller bandwidths are more efficient to solve for less computations.

Multi-resolution grid blocks require tailored ordering schemes due to the complexity of the grids. Parashar *et al*. (1997) have used dynamic locally adaptive mesh refinements for developing parallel reservoir simulators [4]. Wheeler *et al*. (1999) have applied multi-physics and multi-scale simulation by decomposing the physical domain into blocks according to the geometry, geology, and physics/chemistry of several sub-domains [5]. However, there is a very limited documentation of the ordering schemes used in the available literature in the field of multi-resolution up-scaling [6]. Local grid refinement is an approach used for representing higher resolution areas (e.g. hydraulic fracturing simulated models) using commercial simulation softwares such as Eclipse and CMG [7]. Multi-resolution block-ordering systems presented by Shelton (2008) [8] and Dewar (2007) [9] for aerospace applications are too complex for the purpose of fluid flow simulations in hydrocarbon reservoirs.

Even the unconventional multi-resolution up-scaling methods reported in the literature for fluid flow simulation such as wavelet-based [10-12], and Kernel-based [13, 14] lack any explanations on the block-ordering systems applied.

In this paper, an innovative block-ordering system for wavelet-based up-scaling is presented. In the next sections, the block-ordering, up-scaling, fluid flow simulation, and optimization procedures are explained in detail.

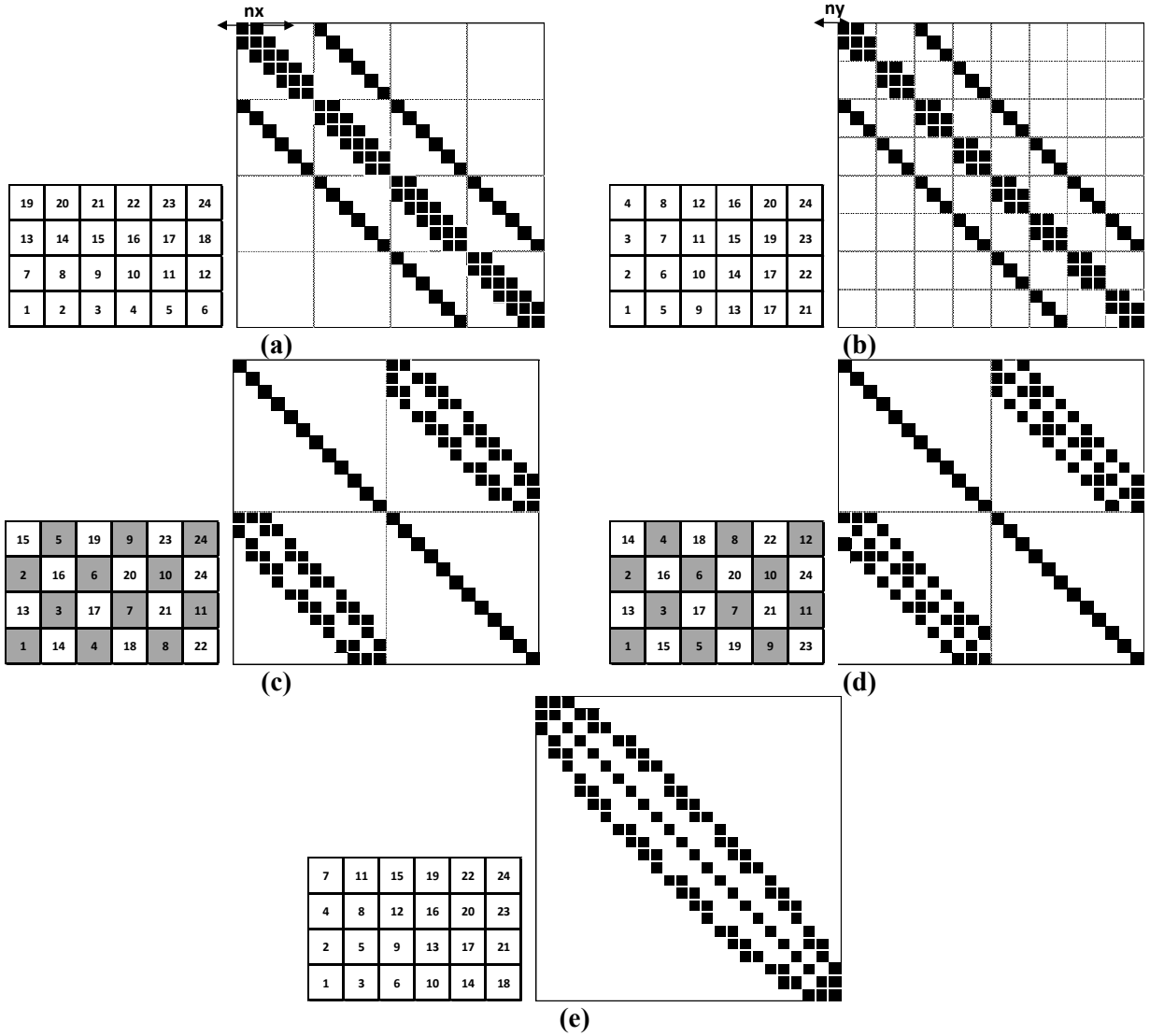

Figure 1. Various block-ordering systems and the resulting coefficient matrices. a) natural ordering by rows, b) natural ordering by columns, c) D-4 ordering, d) cyclic-2 ordering, e) D-2 ordering.

2. Wavelet-based up-scaling methodology

Wavelets are orthogonal functions that represent data in terms of averages and fluctuations. Wavelet methodology is capable of decomposing the fine models into various levels with different frequency bandwidths. It is possible to select various bandwidth coefficients by defining a variability threshold. As a result, cell sizes where variability is high are smaller (higher levels of decomposition) than cell sizes in an area with less variability (lower levels of decomposition). Therefore, it is a good fit for multi-resolution up-scaling purposes.

Equation 1 represents a common mother wavelet [15, 16].

$$\psi_{a_j b_j}(t) = \frac{1}{\sqrt{a_j}} \psi\left(\frac{t - b_j}{a_j}\right) j = 1.2.\ldots.k \quad (1)$$

where $\psi(t)$ is the mother wavelet in time (in our case, location) of t, and a and b are the scale and translation parameters, respectively. The result of a wavelet-based up-scaling technique is a quad-tree multi-resolution network in which averages are numbers assigned to a block and fluctuations are significant features controlling the size of the blocks. More fluctuations result in smaller block sizes.

There are two distinct wavelet-based up-scaling approaches in the literature [17]. The first approach is to apply wavelet transformation to the flow equations to generate a coarsened pressure equation [17-20]. In the second approach, the wavelet filtering procedure is used to reduce the number of data points without compromising the statistics [21-23]. This approach leads to quad-tree (in 2D models) or octree (in 3D models) Cartesian up-scaled grids.

It has been shown by Vahedi *et al*. that there is an inverse relation between the calculation time and the model's error; while functions with a larger number of coefficients for the first level of up-scaling such as Bior 1.3 reduce the flow simulation time, it will increase the error [24]. Conversely, using functions with a smaller number of coefficients (Haar) leads to a higher simulation time with lower error.

In this work, we applied the latter up-scaling approach and used Haar mother wavelet because of its simple form and widespread applications. The Haar mother wavelet is displayed in Figure 2.

$$\psi_{n.k}(t) = 2^{n/2} \psi\left(2^n t - k\right) t \in R \quad (2)$$

where *n* represents the scale factor, k represents translation, t represents the time (in our study, location), and $\psi_{n.k}$ is the Haar function.

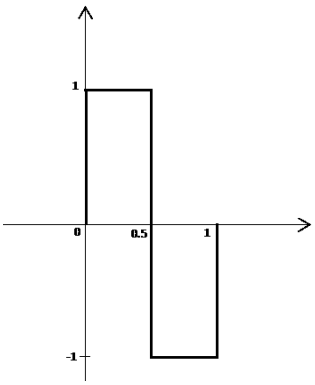

Figure 2. *Haar* mother wavelet.

Equation 3 is the average term of Equation 1 in 2 dimensions, which is reached from tensor multiplication:

$$\varphi_{j,k1,k2}(x, y) = \varphi_j^{k1}(x)\varphi_j^{k2}(y) \quad (3)$$

where φ is the scale function, which is orthogonal to mother wavelet, and its mean is equal to 1:

$$\int_{-\infty}^{+\infty} \varphi(x) dx = 1 \quad (4)$$

Three fluctuations are also achieved in directions *x*, *y,* and *diagonal*. For 2D wavelet based up-scaling, transform has to be applied on data base in one of the directions (for example, *x*), and average has to be achieved (Eq. 1). Then transform equation has to be applied on average coefficients (Eq. 3) in order to reach the final results.

3. Permeability up-scaling in a synthetic heterogeneous reservoir

A synthetic 32 × 32 heterogeneous reservoir is generated, for which, permeability values are shown in Figure 3. Different colored blocks in this figure correspond to wavelet-based multi-resolution up-scaled blocks in Figures 4 and 5.

Standard deviation (SD) and permeability values of the wavelet-based up-scaled blocks are reported in Figures 4 and 5, respectively. SD measures presented in Figure 5 show a high level of variability in the up-scaled blocks with the lowest value of 9.5 md in the largest block and the highest measure of 164.9 md in the finest block. This variability confirms that the heterogeneity of the reservoir is preserved in the multi-resolution up-scaled model.

In order to demonstrate the strength of the applied multi-resolution up-scaling approach in maintaining the variability of a heterogeneous reservoir, a single resolution up-scaling procedure was performed on the dataset given in Figure 3. It should be demonstrated that 31 blocks are resulted from multi-resolution up-scaling (Figure 5). Therefore, it was tried to reach a similar number of blocks in single resolution un-scaling (Figure 6). There are 32× 32 = 1024 fine blocks available (Figure 3). Thus 6 × 6 = 32 fine blocks were merged to reach 29 up-scaled blocks (Figure 6). For example, up-left block in Figure 6 was resulted from merging 6 × 6 up-left blocks in Figure 3. The up-scaled blocks (#29 blocks) and the corresponding SD measures are shown in Figure 6.

313	389	297	312	273	297	327	281	339	295	335	305	298	308	334	373	318	267	279	299	293	296	297	314	292	305	296	295	262	276	273	302
309	369	337	326	280	294	328	309	302	322	307	271	252	285	273	321	249	328	276	280	279	320	305	326	301	274	296	293	289	281	323	301
289	266	335	318	226	308	278	294	263	281	305	271	289	312	324	334	291	309	271	325	272	267	288	272	301	324	287	338	296	287	309	282
267	376	335	292	336	308	302	328	281	265	340	303	255	318	303	274	279	293	287	297	363	242	322	332	321	308	342	294	307	292	299	299
308	318	317	307	308	278	270	273	273	264	280	318	321	343	336	288	261	301	250	282	341	264	266	317	338	303	278	273	293	300	305	306
322	298	270	280	281	299	272	301	359	312	317	365	278	295	251	293	313	293	324	334	308	308	311	298	312	313	288	340	311	224	261	311
244	318	318	322	334	296	300	314	285	296	321	283	303	247	295	327	307	256	313	294	269	310	279	295	295	307	282	331	310	289	298	291
346	295	341	271	257	316	338	328	319	295	294	305	286	279	270	293	301	293	299	285	278	311	292	295	316	276	271	294	269	331	340	294
351	311	325	323	330	238	321	296	308	366	269	407	321	280	387	359	269	315	298	272	338	319	308	344	275	247	354	293	280	288	293	293
244	258	284	315	260	315	283	325	285	404	379	340	325	326	285	326	330	303	214	324	189	300	263	320	288	329	328	339	255	297	298	309
356	312	306	309	299	245	311	247	275	303	296	335	246	251	300	319	338	272	287	349	272	321	291	327	303	284	238	288	346	337	263	254
308	270	276	331	251	242	303	287	335	308	277	251	289	353	325	276	419	290	337	353	344	355	290	307	293	270	311	308	285	278	305	326
325	302	267	323	326	302	321	268	289	241	289	282	293	330	213	270	282	309	327	312	386	274	226	191	308	294	265	317	303	320	279	361
258	316	323	306	322	276	313	290	330	321	257	306	302	286	185	265	303	345	279	337	346	312	350	322	310	264	294	302	314	308	298	324
285	308	300	283	300	310	322	316	382	295	284	309	322	329	216	302	311	295	292	286	340	295	263	300	277	299	304	322	303	294	308	292
293	327	299	284	298	317	297	321	328	288	262	289	363	288	288	268	231	377	287	322	260	220	402	263	296	286	319	308	277	274	277	311
296	301	304	317	291	284	312	292	302	312	306	312	306	300	308	305	320	220	309	370	307	398	215	253	274	286	307	332	293	315	315	320
308	283	297	298	307	302	291	301	292	291	297	291	321	306	313	314	261	181	303	256	205	369	301	339	347	274	312	312	286	303	315	314
323	297	292	298	299	311	297	314	289	302	302	316	302	292	303	325	342	286	334	302	375	301	311	304	324	277	263	329	292	345	245	274
288	292	306	292	305	293	313	301	306	294	313	297	281	290	315	303	303	356	232	282	327	254	351	262	320	295	274	303	273	308	267	310
301	293	301	293	291	289	314	297	306	305	280	287	315	299	310	293	338	330	309	318	288	294	258	265	278	258	289	284	288	345	264	281
287	290	298	291	285	299	307	304	303	300	285	294	312	298	302	307	313	295	322	392	276	271	231	285	308	315	303	263	295	282	310	338
312	301	303	303	307	285	304	298	304	300	304	308	295	311	308	288	288	314	270	285	284	278	275	241	286	297	328	304	301	313	337	299
313	319	309	314	311	300	295	304	292	327	294	310	302	305	302	298	392	304	261	250	323	235	247	299	292	317	293	320	298	293	292	341
285	294	304	305	315	307	307	299	296	294	297	301	307	305	296	302	289	284	262	320	304	306	282	303	317	281	272	328	298	206	416	217
317	297	302	308	286	302	293	300	299	300	287	303	303	287	303	313	315	306	282	303	292	311	256	311	253	227	264	398	277	298	289	320
290	310	303	312	288	283	305	304	294	324	292	306	306	291	300	313	298	275	285	314	297	285	323	303	355	283	242	409	304	240	320	325
302	311	300	278	287	295	303	312	303	290	296	287	299	302	297	300	249	324	310	310	315	307	322	370	222	235	199	276	255	207	358	304
310	304	293	298	300	297	310	304	321	305	293	295	300	297	316	308	275	284	324	275	326	315	298	271	412	311	380	104	308	261	275	313
301	309	307	303	294	316	296	315	296	290	292	284	301	312	302	297	315	345	308	319	295	302	322	254	186	404	371	302	274	336	320	269
321	308	313	306	312	308	306	282	306	309	296	296	293	312	325	306	299	273	291	284	308	343	305	271	248	361	486	248	335	383	353	331
325	297	295	288	287	299	307	296	291	303	292	309	313	295	297	317	272	305	320	285	294	285	307	273	154	139	98	359	258	281	347	296

Figure 3. Permeability (md) value distribution in the synthetic heterogeneous reservoir.

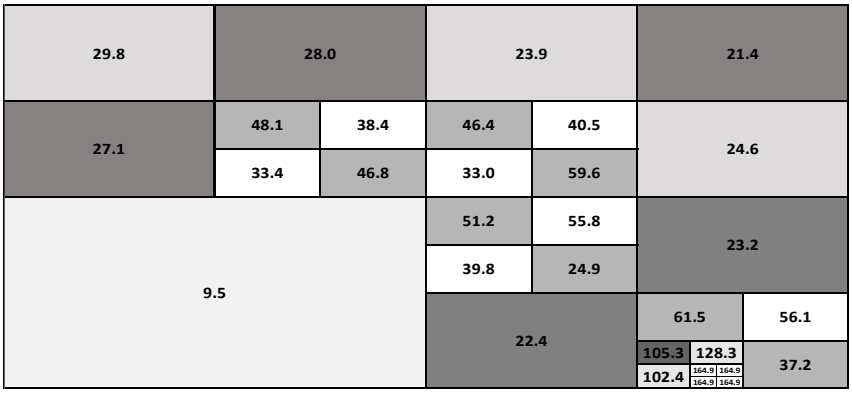

Figure 4. Standard deviation of the permeability values in the wavelet-based up-scaled blocks.

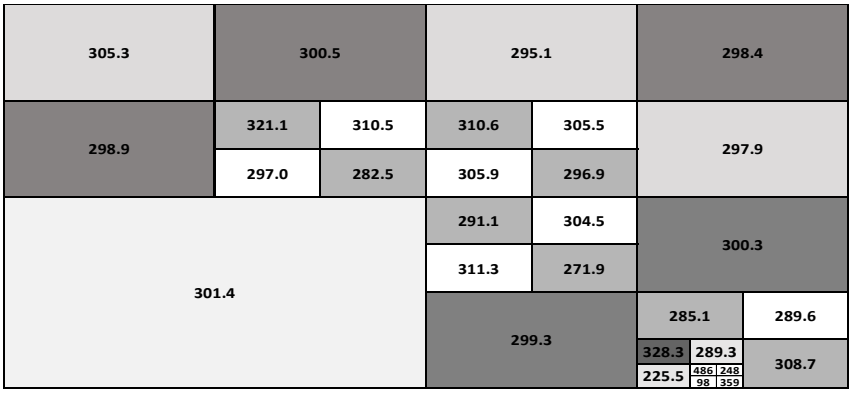

Figure 5. Permeability values of the wavelet-based up-scaled blocks.

32.1	27.5	28.8	27.0	23.1	21.4
34.9	36.2	37.4	35.1	27.6	
16.6	24.3	44.9	53.0	18.7	
9.8	9.5	21.4	38.0	21.4	39.9
9.8	9.1	15.9	22.5	69.0	
12.5			79.9		

Figure 6. Standard deviation of permeability in single resolution up-scaled grid block.

A comparison between multi-resolution up-scaled models (Figure 5) and single resolution up-scaled models (Figure 6) demonstrates how variability is preserved in the multi-resolution up-scaled model:

Original variance of permeability	1061
Weighted average of variance in the wavelet-based up-scaled model	1091
Weighted average of variance in the single resolution up-scaled model	1126

4. Proposed block-ordering system

This section outlines the step by step procedure for the proposed ordering system in the multi-resolution grid block:

1. Sort all blocks in an ascending order first by their center point's 'Y' coordinates and then by their 'X' coordinates, and assign labels accordingly (Figure 7).
2. Calculate **dx** (distance in X direction) and **dy** (distance in Y direction) for adjoining blocks with similar Y coordinates.
3. Select the smallest blocks (based on their **dx** and **dy**) and calculate the coordinates of their corner points using the following operations:

$$x_{min} = x_{center} - \left(\frac{dx}{2}\right)_{min} \quad (5)$$

$$x_{max} = x_{center} + \left(\frac{dx}{2}\right)_{min} \quad (6)$$

$$y_{min} = y_{center} - \left(\frac{dy}{2}\right)_{min} \quad (7)$$

$$y_{max} = y_{center} + \left(\frac{dy}{2}\right)_{min} \quad (8)$$

4. Merge all four neighboring blocks with minimum **dx** (Figure 8). Calculate the coordinates for the center of merged block and label this block by adding one to the largest block number in the model.
5. Repeat steps 3 and 4, and calculate the coordinates of the merged blocks (Figures 9, 10, and 11).

The 16 blocks in Figure 10 will be merged into four blocks. In situations where more than one set of four blocks are to be merged, labeling will be done based on the X and Y coordinates of the sets, starting from the smallest.

6. At each step, coordinates of the corner points of all blocks will be saved in a matrix with size N*4, in which N is the number of blocks. Table 1 shows the calculated coordinates of the block corner points in Figure 7.
7. Calculate intersections between neighboring blocks in Figure 7, in 'X' (Table 2) and 'Y' (Table 3) direction. For example, block 1 in Figure 7 has an 'X' sideway intersection with block 4 (Table 3) and two 'Y' sideway intersections with blocks 2 and 3 (Table 4).

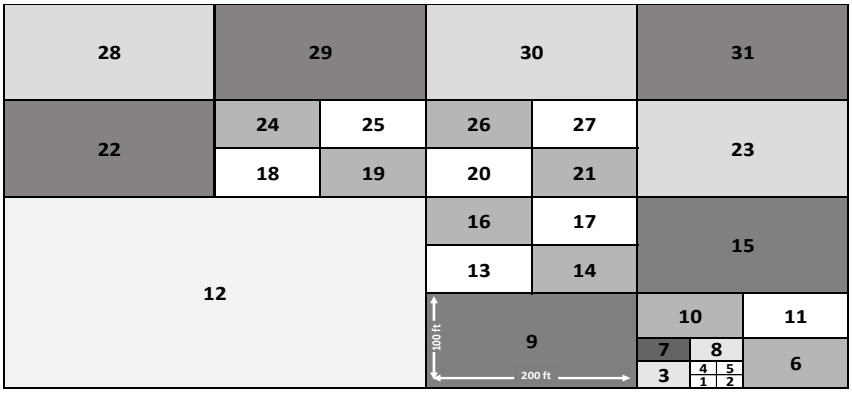

Figure 7. Labeling the multi-resolution blocks using the developed procedure.

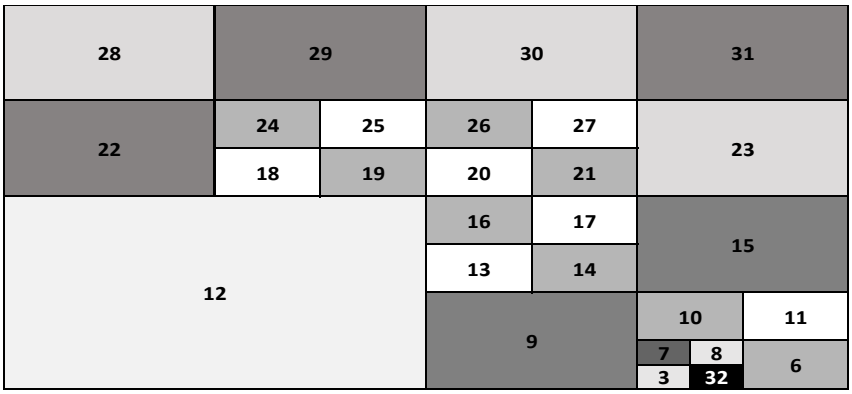

Figure 8. Merging the smallest blocks and re-labeling the merged blocks (showed in black) (first iteration).

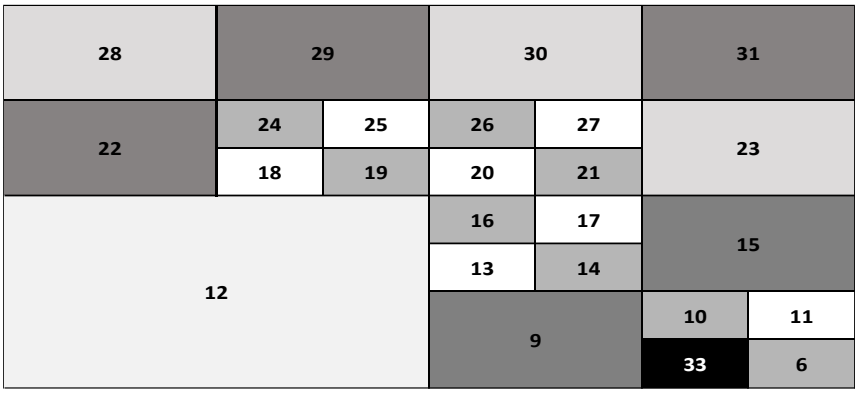

Figure 9. Merging the smallest block and re-labeling the merged blocks (showed in black) (second iteration).

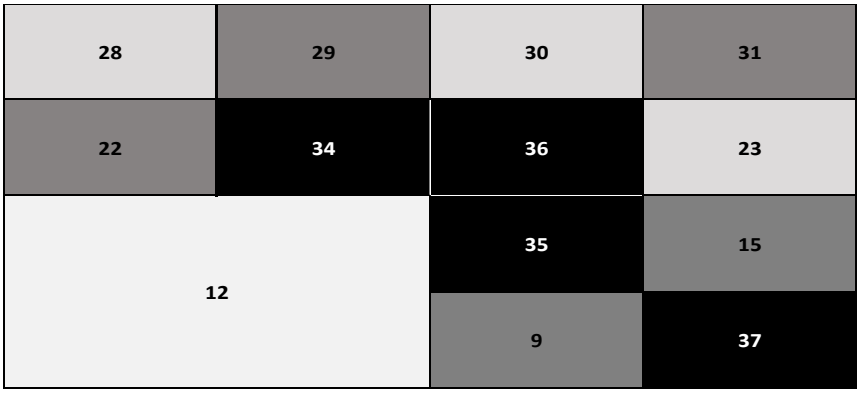

Figure 10. Merging of the smallest block and re-labeling the merged blocks (showed in black) (third iteration).

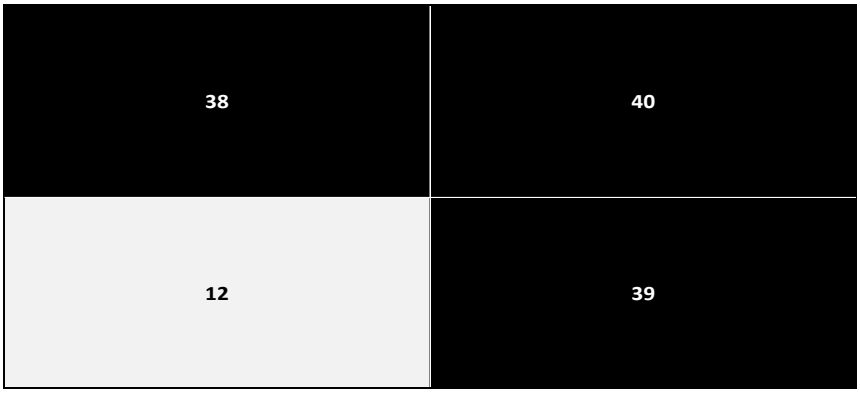

Figure 11. Merging of the smallest block and re-labeling the merged blocks (showed in black) (fourth iteration).

Table 1. Calculated coordinates of the corner points of all blocks.

Block	X_{min}	X_{max}	Y_{min}	Y_{max}
1	650	675	0	12.5
2	675	700	0	12.5
3	600	650	0	25
4	650	675	12.5	25
5	675	700	12.5	25
6	700	800	0	50
7	600	650	25	50
8	650	700	25	50
9	400	600	0	100
10	600	700	50	100
11	700	800	50	100
12	0	400	0	200
13	400	500	100	150
14	500	600	100	150
15	600	800	100	200
16	400	500	150	200
17	500	600	150	200
18	200	300	200	250
19	300	400	200	250
20	400	500	200	250
21	500	600	200	250
22	0	200	200	300
23	600	800	200	300
24	200	300	250	300
25	300	400	250	300
26	400	500	250	300
27	500	600	250	300
28	0	200	300	400
29	200	400	300	400
30	400	600	300	400
31	600	800	300	400

Table 2. Calculated intersections of the blocks in Figure 7 in 'X' direction.

	1	2	3	4	5	6	7	8	9	10	11	12	13	14	15	16	17	18	19	20	21	22	23	24	25	26	27	28	29	30	31
1	0	0	0	25	0	0	0	0	0	0	0	0	0	0	0	0	0	0	0	0	0	0	0	0	0	0	0	0	0	0	0
2	0	0	0	0	25	0	0	0	0	0	0	0	0	0	0	0	0	0	0	0	0	0	0	0	0	0	0	0	0	0	0
3	0	0	0	0	0	0	50	0	0	0	0	0	0	0	0	0	0	0	0	0	0	0	0	0	0	0	0	0	0	0	0
4	25	0	0	0	0	0	0	25	0	0	0	0	0	0	0	0	0	0	0	0	0	0	0	0	0	0	0	0	0	0	0
5	0	25	0	0	0	0	0	25	0	0	0	0	0	0	0	0	0	0	0	0	0	0	0	0	0	0	0	0	0	0	0
6	0	0	0	0	0	0	0	0	0	100	0	0	0	0	0	0	0	0	0	0	0	0	0	0	0	0	0	0	0	0	0
7	0	0	50	0	0	0	0	0	0	50	0	0	0	0	0	0	0	0	0	0	0	0	0	0	0	0	0	0	0	0	0
8	0	0	0	25	25	0	0	0	0	50	0	0	0	0	0	0	0	0	0	0	0	0	0	0	0	0	0	0	0	0	0
9	0	0	0	0	0	0	0	0	0	0	0	0	100	100	0	0	0	0	0	0	0	0	0	0	0	0	0	0	0	0	0
10	0	0	0	0	0	0	50	50	0	0	0	0	0	0	100	0	0	0	0	0	0	0	0	0	0	0	0	0	0	0	0
11	0	0	0	0	0	100	0	0	0	0	0	0	0	0	100	0	0	0	0	0	0	0	0	0	0	0	0	0	0	0	0
12	0	0	0	0	0	0	0	0	0	0	0	0	0	0	0	0	0	100	100	0	0	200	0	0	0	0	0	0	0	0	0
13	0	0	0	0	0	0	0	0	100	0	0	0	0	0	0	100	0	0	0	0	0	0	0	0	0	0	0	0	0	0	0
14	0	0	0	0	0	0	0	0	100	0	0	0	0	0	0	0	100	0	0	0	0	0	0	0	0	0	0	0	0	0	0
15	0	0	0	0	0	0	0	0	0	100	100	0	0	0	0	0	0	0	0	0	0	200	0	0	0	0	0	0	0	0	0
16	0	0	0	0	0	0	0	0	0	0	0	0	100	0	0	0	0	0	0	100	0	0	0	0	0	0	0	0	0	0	0
17	0	0	0	0	0	0	0	0	0	0	0	0	0	100	0	0	0	0	0	0	100	0	0	0	0	0	0	0	0	0	0
18	0	0	0	0	0	0	0	0	0	0	0	100	0	0	0	0	0	0	0	0	0	0	0	100	0	0	0	0	0	0	0
19	0	0	0	0	0	0	0	0	0	0	0	100	0	0	0	0	0	0	0	0	0	0	0	0	100	0	0	0	0	0	0
20	0	0	0	0	0	0	0	0	0	0	0	0	0	0	0	100	0	0	0	0	0	0	0	0	0	100	0	0	0	0	0
21	0	0	0	0	0	0	0	0	0	0	0	0	0	0	0	0	100	0	0	0	0	0	0	0	0	0	100	0	0	0	0
22	0	0	0	0	0	0	0	0	0	0	0	200	0	0	0	0	0	0	0	0	0	0	0	0	0	0	0	200	0	0	0
23	0	0	0	0	0	0	0	0	0	0	0	0	0	0	200	0	0	0	0	0	0	0	0	0	0	0	0	0	0	0	200
24	0	0	0	0	0	0	0	0	0	0	0	0	0	0	0	0	0	100	0	0	0	0	0	0	0	0	0	0	100	0	0
25	0	0	0	0	0	0	0	0	0	0	0	0	0	0	0	0	0	0	100	0	0	0	0	0	0	0	0	0	100	0	0
26	0	0	0	0	0	0	0	0	0	0	0	0	0	0	0	0	0	0	0	100	0	0	0	0	0	0	0	0	0	100	0
27	0	0	0	0	0	0	0	0	0	0	0	0	0	0	0	0	0	0	0	0	100	0	0	0	0	0	0	0	0	100	0
28	0	0	0	0	0	0	0	0	0	0	0	0	0	0	0	0	0	0	0	0	0	200	0	0	0	0	0	0	0	0	0
29	0	0	0	0	0	0	0	0	0	0	0	0	0	0	0	0	0	0	0	0	0	0	0	100	100	0	0	0	0	0	0
30	0	0	0	0	0	0	0	0	0	0	0	0	0	0	0	0	0	0	0	0	0	0	0	0	0	100	100	0	0	0	0
31	0	0	0	0	0	0	0	0	0	0	0	0	0	0	0	0	0	0	0	0	0	0	200	0	0	0	0	0	0	0	0

5. Fluid flow simulation

Block pressure (P) for all blocks can be calculated using the following equation:

$$\underline{\underline{A}} * \underline{P} = \underline{B} \tag{9}$$

where $\underline{\underline{A}}$ is the N x N matrix of transmissibility, N is the number of blocks (equal to 31 in the current example), $\underline{P}$ represents a vector of unknown block pressures that will be optimized later, and $\underline{B}$ represents the vector of boundary condition.

Equations used for calculating the related elements in matrix $\underline{\underline{A}}$ are as follow [2, 3, 25]:

$$E_{i+\frac{1}{2}.j} = T^{n}_{x_{i+\frac{1}{2}.j}} = \left[\frac{2\beta c}{\frac{\mu_i B_{o.i} \Delta x_i}{k_{x_i} \Delta y_i \Delta z_i} + \frac{\mu_{i+1} B_{o.i+1} \Delta x_{i+1}}{k_{x_{i+1}} IntSecy_{i+1} \Delta z_{i+1}}} \right]^{n}_{j} \tag{10}$$

$$W_{i-\frac{1}{2}.j} = T^{n}_{x_{i-\frac{1}{2}.j}} = \left[\frac{2\beta_c}{\frac{\mu_{i-1} B_{o.i-1} \Delta x_{i-1}}{k_{x_{i-1}} IntSecy_{i-1} \Delta z_{i-1}} + \frac{\mu_i B_{o.i} \Delta x_i}{k_{x_i} \Delta y_i \Delta z_i}} \right]^{n}_{j} \tag{11}$$

$$N_{i.j+\frac{1}{2}} = T^{n}_{y_{i.j+\frac{1}{2}}} = \left[\frac{2\beta_c}{\frac{\mu_j B_{o.j} \Delta y_j}{k_{x_j} \Delta x_j \Delta z_j} + \frac{\mu_{j+1} B_{o.j+1} \Delta y_{j+1}}{k_{x_{j+1}} IntSecx_{j+1} \Delta z_{j+1}}} \right]^{n}_{i} \tag{12}$$

$$S_{i.j-\frac{1}{2}} = T^{n}_{y_{i.j-\frac{1}{2}}} = \left[\frac{2\beta_c}{\frac{\mu_{j-1} B_{o.j-1} \Delta y_{j-1}}{k_{x_{j-1}} IntSecx_{j-1} \Delta z_{j-1}} + \frac{\mu_j B_{o.j} \Delta y_j}{k_{x_j} \Delta x_j \Delta z_j}} \right]^{n}_{i} \tag{13}$$

where β_c is a unit coefficient (in this case, equal to 0.001127); μ_i, $B_{o,i}$, and k_{x_i} are the viscosity, formation volume factor, and permeability of block i, respectively; Δx_i, Δy_i, and Δz_i correspond to the block sizes in directions x, y, and z. $IntSecy_{i+1}$ and $IntSecy_{i-1}$ are intersections between two blocks in direction 'Y' (extracted from Table 3). $IntSecx_{j+1}$ and $IntSecx_{j-1}$ are intersections between two blocks in direction 'X' (extracted from Table 2). $T^{n}_{x_{i+\frac{1}{2}.j}}$ is transmissibility between a block and its right hand side neighbor block (e.g. transmissibility from block 12 to 13). $T^{n}_{x_{i-\frac{1}{2}.j}}$ is transmissibility between a block and its left hand side neighbor block (e.g. transmissibility from block 13 to 12). $T^{n}_{y_{i.j+\frac{1}{2}}}$ is transmissibility between a block and the neighboring block directly above it (transmissibility from block 12 to 22). $T^{n}_{y_{i.j-\frac{1}{2}}}$ is transmissibility between a block and the neighboring block directly below it (transmissibility from block 22 to 12).

Transmissibility in each block (diagonal elements in matrix $\underline{\underline{A}}$) is calculated using Equation 14:

$$T^{n}_{i.j} = -\left[E^{n}_{i.j} + W^{n}_{i.j} + N^{n}_{i.j} + S^{n}_{i.j} + \frac{\Pi^{n+1}_{i.j}}{\Delta t} \right] \qquad i = j \tag{14}$$

where Δt is the prediction time between steps n and n+1. $\Pi^{n+1}_{i.j}$ is calculated using Equation 15:

$$\Pi^{n+1}_{i.j} = \left(\frac{V_b \varphi Co}{\alpha_c B_{oRef}} \right)^{n}_{i.j} \tag{15}$$

in which V_b is the volume of each block (dx.dy.dz), φ is the porosity of each block, α_c is a constant (in this case, equal to 5.615), and B_{oRef} is the formation volume factor for each block. Co is the total oil compressibility calculated using Equation 16:

$$Co = Sw_{i.j} Cw_{i.j} + (1 - Sw_{i.j}) Co_{i.j} + Cr_{i.j} \tag{16}$$

Synthetic reservoir's characteristics are shown in Table 4. Transmissibility of the blocks in Figure 4, calculated based on these characteristics, are reported in Table 5.

It was explained earlier that bandwidth expressed as $2 \times n_i + 1$ is the maximum number of elements within the band envelop in any row of the matrix. By this definition, the maximum bandwidth in the coefficient matrix shown in Table 5 happens in rows 22 and 23, and is equal to 16. To take advantage of the fact that smaller bandwidths result in fewer computations, block-ordering should be done in whichever direction that results in a coefficient matrix with a smaller bandwidth. If the blocks in Figure 3 were labeled based on minimum *dx,* as shown in Figure 12, the resulting coefficient matrix would have a maximum bandwidth of 18. Therefore, in this example, ordering of the blocks based on minimum *dy,* which resulted in a smaller bandwidth, and hence, less computation time, is the preferred direction for labelling.

Vector $\underline{B}$ in Equation 9 is calculated using the following equation:

$$Q^{n}_{i.j} = -\left[\frac{\Pi^{n+1}_{i.j}}{\Delta t} P^{n}_{i.j} + q^{n}_{osc_{i.j}} \right] \qquad i = j \tag{17}$$

where $P^{n}_{i.j}$ and $q^{n}_{osc_{i.j}}$ are pressure and oil injection/production in each block (as shown in Table 4). The calculated values for vector $\underline{B}$ are reported in Table 6.

Table 3. Calculated intersections of the blocks in Figure 7 in 'Y' direction.

	1	2	3	4	5	6	7	8	9	10	11	12	13	14	15	16	17	18	19	20	21	22	23	24	25	26	27	28	29	30	31
1	0	12.5	12.5	0	0	0	0	0	0	0	0	0	0	0	0	0	0	0	0	0	0	0	0	0	0	0	0	0	0	0	0
2	12.5	0	0	0	0	12.5	0	0	0	0	0	0	0	0	0	0	0	0	0	0	0	0	0	0	0	0	0	0	0	0	0
3	12.5	0	0	12.5	0	0	0	0	25	0	0	0	0	0	0	0	0	0	0	0	0	0	0	0	0	0	0	0	0	0	0
4	0	0	12.5	0	12.5	0	0	0	0	0	0	0	0	0	0	0	0	0	0	0	0	0	0	0	0	0	0	0	0	0	0
5	0	0	0	12.5	0	12.5	0	0	0	0	0	0	0	0	0	0	0	0	0	0	0	0	0	0	0	0	0	0	0	0	0
6	0	12.5	0	0	12.5	0	0	25	0	0	0	0	0	0	0	0	0	0	0	0	0	0	0	0	0	0	0	0	0	0	0
7	0	0	0	0	0	0	0	25	25	0	0	0	0	0	0	0	0	0	0	0	0	0	0	0	0	0	0	0	0	0	0
8	0	0	0	0	0	25	25	0	0	0	0	0	0	0	0	0	0	0	0	0	0	0	0	0	0	0	0	0	0	0	0
9	0	0	25	0	0	0	25	0	0	50	0	100	0	0	0	0	0	0	0	0	0	0	0	0	0	0	0	0	0	0	0
10	0	0	0	0	0	0	0	0	50	0	50	0	0	0	0	0	0	0	0	0	0	0	0	0	0	0	0	0	0	0	0
11	0	0	0	0	0	0	0	0	0	50	0	0	0	0	0	0	0	0	0	0	0	0	0	0	0	0	0	0	0	0	0
12	0	0	0	0	0	0	0	0	100	0	0	0	50	0	0	50	0	0	0	0	0	0	0	0	0	0	0	0	0	0	0
13	0	0	0	0	0	0	0	0	0	0	0	50	0	50	0	0	0	0	0	0	0	0	0	0	0	0	0	0	0	0	0
14	0	0	0	0	0	0	0	0	0	0	0	50	0	50	0	0	0	0	0	0	0	0	0	0	0	0	0	0	0	0	0
15	0	0	0	0	0	0	0	0	0	0	0	0	50	0	0	50	0	0	0	0	0	0	0	0	0	0	0	0	0	0	0
16	0	0	0	0	0	0	0	0	0	0	50	0	0	0	0	50	0	0	0	0	0	0	0	0	0	0	0	0	0	0	0
17	0	0	0	0	0	0	0	0	0	0	0	0	0	0	50	50	0	0	0	0	0	0	0	0	0	0	0	0	0	0	0
18	0	0	0	0	0	0	0	0	0	0	0	0	0	0	0	0	0	50	0	0	50	0	0	0	0	0	0	0	0	0	0
19	0	0	0	0	0	0	0	0	0	0	0	0	0	0	0	0	0	50	0	50	0	0	0	0	0	0	0	0	0	0	0
20	0	0	0	0	0	0	0	0	0	0	0	0	0	0	0	0	0	50	0	50	0	0	0	0	0	0	0	0	0	0	0
21	0	0	0	0	0	0	0	0	0	0	0	0	0	0	0	0	0	0	50	0	50	0	0	0	0	0	0	0	0	0	0
22	0	0	0	0	0	0	0	0	0	0	0	0	0	0	0	0	0	50	0	0	0	50	0	0	0	0	0	0	0	0	0
23	0	0	0	0	0	0	0	0	0	0	0	0	0	0	0	0	0	0	0	50	0	0	50	0	0	50	0	0	0	0	0
24	0	0	0	0	0	0	0	0	0	0	0	0	0	0	0	0	0	0	0	0	50	0	0	50	0	0	0	0	0	0	0
25	0	0	0	0	0	0	0	0	0	0	0	0	0	0	0	0	0	0	0	0	0	50	0	0	50	0	0	0	0	0	0
26	0	0	0	0	0	0	0	0	0	0	0	0	0	0	0	0	0	0	0	0	0	0	50	0	0	50	0	0	0	0	0
27	0	0	0	0	0	0	0	0	0	0	0	0	0	0	0	0	0	0	0	0	0	0	0	50	0	0	50	0	0	0	0
28	0	0	0	0	0	0	0	0	0	0	0	0	0	0	0	0	0	0	0	0	0	0	0	0	0	0	0	0	100	0	0
29	0	0	0	0	0	0	0	0	0	0	0	0	0	0	0	0	0	0	0	0	0	0	0	0	0	0	0	100	0	100	0
30	0	0	0	0	0	0	0	0	0	0	0	0	0	0	0	0	0	0	0	0	0	0	0	0	0	0	0	0	100	0	100
31	0	0	0	0	0	0	0	0	0	0	0	0	0	0	0	0	0	0	0	0	0	0	0	0	0	0	0	0	0	100	0

Table 4. Synthetic reservoir characteristics.

Permeability (md)	Randomly generated ($\mu = 315$, $\sigma = 5$)
Porosity	0.27%
Initial Pressure (psi)	4000 psi
S_w	1.0
C_w	1.00E-06
C_r and C_o	0.0
Formation Volume Factor	1.0
Viscosity	0.5
Dz (ft)	40
Boundary Condition (qB)	0.0, except in block 1: 4000 psi
q_{osc} (source/sink)	0.0, except in block 9 with a well producing at 600 bl/day

Table 5. Rounded transmissibility of the blocks in Figure 7.

	1	2	3	4	5	6	7	8	9	10	11	12	13	14	15	16	17	18	19	20	21	22	23	24	25	26	27	28	29	30	31
1	-27	22	1	4	0	0	0	0	0	0	0	0	0	0	0	0	0	0	0	0	0	0	0	0	0	0	0	0	0	0	0
2	9	-19	0	0	9	1	0	0	0	0	0	0	0	0	0	0	0	0	0	0	0	0	0	0	0	0	0	0	0	0	0
3	6	0	-57	14	0	0	34	0	2	0	0	0	0	0	0	0	0	0	0	0	0	0	0	0	0	0	0	0	0	0	0
4	4	0	1	-41	20	0	0	16	0	0	0	0	0	0	0	0	0	0	0	0	0	0	0	0	0	0	0	0	0	0	0
5	0	9	0	29	-52	1	0	12	0	0	0	0	0	0	0	0	0	0	0	0	0	0	0	0	0	0	0	0	0	0	0
6	0	15	0	0	12	-95	0	14	0	0	54	0	0	0	0	0	0	0	0	0	0	0	0	0	0	0	0	0	0	0	0
7	0	0	5	0	0	0	-52	18	2	28	0	0	0	0	0	0	0	0	0	0	0	0	0	0	0	0	0	0	0	0	0
8	0	0	0	24	16	2	19	-86	0	26	0	0	0	0	0	0	0	0	0	0	0	0	0	0	0	0	0	0	0	0	0
9	0	0	1	0	0	0	3	0	-44	3	0	2	18	16	0	0	0	0	0	0	0	0	0	0	0	0	0	0	0	0	0
10	0	0	0	0	0	0	38	35	3	-141	13	0	0	0	53	0	0	0	0	0	0	0	0	0	0	0	0	0	0	0	0
11	0	0	0	0	0	12	0	0	0	13	-78	0	0	0	53	0	0	0	0	0	0	0	0	0	0	0	0	0	0	0	0
12	0	0	0	0	0	0	0	0	2	0	0	-702	3	0	0	3	0	95	165	0	0	433	0	0	0	0	0	0	0	0	0
13	0	0	0	0	0	0	0	0	16	0	0	3	-57	21	0	16	0	0	0	0	0	0	0	0	0	0	0	0	0	0	0
14	0	0	0	0	0	0	0	0	14	0	0	0	24	-55	3	0	14	0	0	0	0	0	0	0	0	0	0	0	0	0	0
15	0	0	0	0	0	0	0	0	0	92	93	0	0	3	-623	0	3	0	0	0	0	0	432	0	0	0	0	0	0	0	0
16	0	0	0	0	0	0	0	0	0	0	0	3	16	0	0	-104	13	0	0	71	0	0	0	0	0	0	0	0	0	0	0
17	0	0	0	0	0	0	0	0	0	0	0	0	0	14	3	13	-43	0	0	0	12	0	0	0	0	0	0	0	0	0	0
18	0	0	0	0	0	0	0	0	0	0	0	54	0	0	0	0	0	-84	13	0	0	4	0	13	0	0	0	0	0	0	0
19	0	0	0	0	0	0	0	0	0	0	0	71	0	0	0	0	0	9	-228	9	0	0	0	0	140	0	0	0	0	0	0
20	0	0	0	0	0	0	0	0	0	0	0	0	0	0	0	71	0	0	9	-237	9	0	0	0	0	148	0	0	0	0	0
21	0	0	0	0	0	0	0	0	0	0	0	0	0	0	0	0	12	0	0	24	-52	0	4	0	0	0	11	0	0	0	0
22	0	0	0	0	0	0	0	0	0	0	0	201	0	0	0	0	0	1	0	0	0	-308	0	1	0	0	0	106	0	0	0
23	0	0	0	0	0	0	0	0	0	0	0	0	0	0	200	0	0	0	0	0	1	0	-401	0	0	0	1	0	0	0	199
24	0	0	0	0	0	0	0	0	0	0	0	0	0	0	0	0	0	13	0	0	0	4	0	-54	25	0	0	0	11	0	0
25	0	0	0	0	0	0	0	0	0	0	0	0	0	0	0	0	0	0	140	0	0	0	0	6	-200	6	0	0	48	0	0
26	0	0	0	0	0	0	0	0	0	0	0	0	0	0	0	0	0	0	0	148	0	0	0	0	6	-245	6	0	0	86	0
27	0	0	0	0	0	0	0	0	0	0	0	0	0	0	0	0	0	0	0	0	11	0	4	0	0	19	-70	0	0	36	0
28	0	0	0	0	0	0	0	0	0	0	0	0	0	0	0	0	0	0	0	0	0	98	0	0	0	0	0	-111	14	0	0
29	0	0	0	0	0	0	0	0	0	0	0	0	0	0	0	0	0	0	0	0	0	0	0	13	87	0	0	14	-127	13	0
30	0	0	0	0	0	0	0	0	0	0	0	0	0	0	0	0	0	0	0	0	0	0	0	0	0	144	44	0	9	-206	9
31	0	0	0	0	0	0	0	0	0	0	0	0	0	0	0	0	0	0	0	0	0	0	172	0	0	0	0	0	0	9	-181

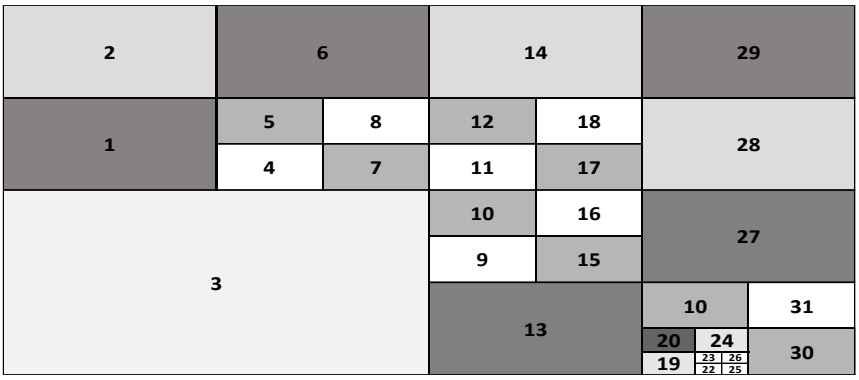

Figure 12. Re-labeling of the up-scaled blocks based on minimum 'X'.

Table 6. Calculated values for vector $\underline{B}$.

Block (i)	B_i
1	-92214.0
2	-40317.5
3	-193416.6
4	-136161.8
5	-92225.7
6	-318159.5
7	-168403.8
8	-137232.1
9	-148118.7
10	-250907.4
11	-230679.8
12	-2407301.9
13	-170312.1
14	-115509.7
15	-1522922.7
16	-328609.1
17	-114422.8
18	-261669.2
19	-704664.6
20	-613163
21	-154698
22	-534817.9
23	-704438.6
24	-174785.8
25	-306070.9
26	-393609.4
27	-224253.8
28	-124400.2
29	-112726.2
30	-82513.1
31	-2061.8

6. Solver: Gaussian elimination

In the previous sections, the procedures for developing the coefficient matrix $\underline{\underline{A}}$ (Table 5) and vector $\underline{B}$ were explained. To solve the resulting system of equations, Gaussian Elimination, which is a simple and fast optimization method, was used. The Gaussian elimination procedure can be described by the following simple steps [26, 27]:

1. Define augmented matrix of $\underline{\underline{A}}$ denoted as $\underline{\underline{\tilde{A}}}$ by including $\underline{B}$ into $\underline{\underline{A}}$ as the last column:

$$\underline{\underline{\tilde{A}}} = \begin{bmatrix} a_{11}a_{12}\ldots a_{1N} & b_1 \\ a\ a_{22}\ldots a_{2N} & b_2 \\ \ldots & \ldots \\ a_{N1}a_{N2}\ldots a_{NN} & b_N \end{bmatrix} \quad (18)$$

2. Convert linear system $\underline{\underline{A}} * \underline{P} = \underline{B}$ to another linear system $\underline{\underline{A}}' * \underline{P} = \underline{B}'$, whose augmented matrix $\underline{\underline{\tilde{A}}}$ is in row echelon form. $\underline{\underline{\tilde{A}}}$ is in row

echelon form if it satisfies the following condition:

- For $i \in [1.N-1]$, the leftmost non-zero element of i^{th} row is at a column that is strictly to the left of the column containing the leftmost non-zero element of the $(i+1)^{th}$ row. For example, matrix $\begin{bmatrix}1234\\0567\\0089\end{bmatrix}$ is in row echelon. In order to convert $\underline{\underline{\tilde{A}}}$ to row echelon form, the following three operations should be done:

1. Switch two rows of $\underline{\underline{\tilde{A}}}$.
2. Multiply all numbers of a row by the same non-zero value.
3. Suppose that $\underline{a_i}$ and $\underline{a_j}$ are two vectors of $\underline{\underline{\tilde{A}}}$. Update row $\underline{a_i}$ to $\underline{a_i} + c\underline{a_j}$, where c can be any real value.

Any matrix $\underline{\underline{\tilde{A}}}$ can be converted into a matrix in row echelon form by performing the above three steps.

3. Now solve the N^{th} row of $\underline{\underline{\tilde{A}}}$ in order to calculate N^{th} $\underline{P}$. Then substitute N^{th} $\underline{P}$ in $(N-1)^{th}$ row in order to calculate $(N-1)^{th}$ $\underline{P}$. Repeat the back-substitute procedure to obtain a unique solution for $\underline{P}$.

Equation $\underline{\underline{A}} * \underline{P} = \underline{B}$ is solved using the Gaussian elimination method. Figure 13 shows the results of pressure simulation in all blocks after one-day of production.

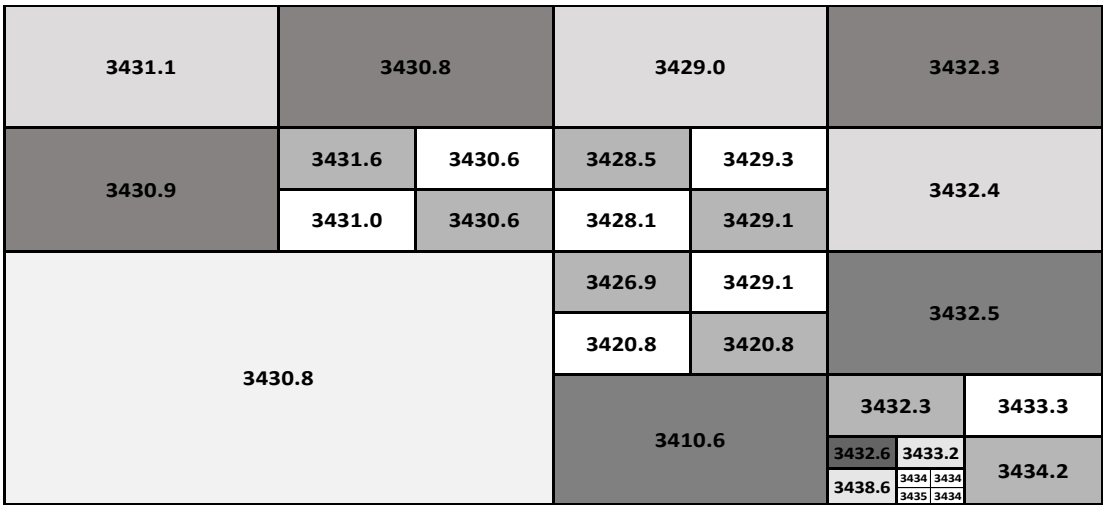

Figure 13. Calculated pressures for the blocks in Figure 8 after one day of production.

7. Conclusions

Very limited attempts have been made for block-ordering procedures in multi-resolution up-scaled reservoir simulations. The developed approaches in other disciplines such as aerospace are usually too complex and not usable in reservoir simulations. In this study, a simple, generalized block-ordering scheme for multi-resolution up-scaling was introduced and explained in detail. The procedure for implementing this ordering scheme for developing the coefficient matrix and solving the linear system of equations was described step by step using a synthetically generated grid block. It was shown that how using this block-ordering scheme could result in a coefficient matrix with a smaller bandwidth with optimized CPU processing time. The developed methodology will help in adapting different block sizes for the grid block; fine grids will be used for areas with high variability and coarse grids for areas that show a smooth change in properties. Preserving the variability of the properties in the reservoir model will increase the accuracy of the fluid flow in reservoir simulations.

References

[1]. Ertekin, T., Abou-Kassem, J.H. and King, G.R. (2001). Basic Applied Reservoir Simulation, Henry L. Doherty Memorial Found of AIME, Society of Petroleum Engineers, Richardson, Texas. 406 P.

[2]. Aziz, K. and Settari, A. (1979). Petroleum Reservoir Simulation, Applied Sciences Publisher Ltd., London.

[3]. Abou-Kassem, J.H., Farouq-Ali, S.M. and Islam, M.R. (2006). Petroleum Reservoir Simulation, Gulf Publishing Company. 445 P.

[4]. Parashar, M., Wheeler, J.A., Pope, G., Wang, K. and Wang, P. (1997). A New Generation EOS Compositional Reservoir Simulator: Part II-Framework and Multiprocessing. SPE 37977. 8 P.

[5]. Wheeler, M.F., Arbogast, T., Bryant, S., Eaton, J., Lu, Q., Peszynska, M. and Yotov, I. (1999). A Parallel Multiblock/Multidomain Approach for Reservoir Simulation, SPE 51884. 11 P.

[6]. Keilegavlen, E. (2009). Robust Control Volume Methods for Reservoir Simulation on Challenging Grids, Ph.D. Dissertation, University of Bergen. 120 P.

[7]. Pancaldi, V., King, P. and Christensen, K. (2008). Wavelet-based upscaling of advection equations, Physica A. 387: 4760-4770.

[8]. Shelton, A.B. (2008). A Multi resolution Discontinuous Galerkin Method for Unsteady Compressible Flows, Ph.D. Dissertation, Georgia Institute of Technology. 86 P.

[9]. Dewar, G. (2007). Gray Codes, Universal Cycles and Configuration Orderings for Block Designs, Ph.D. Dissertation, Carleton University. 299 P.

[10]. Rasaei, M.R. and Sahimi, M. (2008). Upscaling and Simulation of Waterflooding in Heterogeneous Reservoirs Using Wavelet Transformations: Application to the SPE-10 Model, Transp. Porous Media. 72: 311-338.

[11]. Ki, S. and Choe, J. (2009). Efficient Contaminant Transport Modeling Using Wavelet-based Conditional Upscaling and Streamline Simulation, Energy Sources, Energy Sources Part A Energy Sources. 31 (10): 843-853.

[12]. Sahimi, M., Darvishi, R., Haghighi, M. and Rasaei, M.R. (2010). Up-scaled Unstructured Computational Grids for Efficient Simulation of Flow in Fractured Porous Media, Transp. Porous Media. 83: 195-218.

[13]. Ebadi, F., Arashi, M. and Tokhmechi, B. (2015). Introducing core estimation variable band width in multi resolution up-scaling of well logs, The Third International Conference of Oil, Gas, Refining & Petrochemical with Focus Relationship between Government, University and Industry, Shiraz, Iran. 8 P.

[14]. Ebadi, F., Arashi, M. and Tokhmechi, B. (2016). A core estimation with variable band width approach in multi resolution up-scaling, The Forth International Conference of Oil, Gas, Refining & Petrochemical with Focus Relationship between Government, University and Industry, Shiraz, Iran. 8 P.

[15]. Daubechies, I. (1990). The wavelet transform, time frequency localization and signal analysis, IEEE Trans. Inform. Theory. 39: 961-1005.

[16]. Daubechies, I. (1990). Ten lectures on wavelets. 268 P.

[17]. Babaei, M. (2013). Multiscale Wavelet and Up-scaling-Downscaling for Reservoir Simulation, Ph.D. Dissertation, Imperial College London. 183 P.

[18]. Pancaldi, V. (2007). Coarse graining equations for ow in porous media: a Haar wavelets and renormalization approach, Ph.D. thesis, Imperial College London. 152 P.

[19]. Pancaldi, V., Christensen, K. and King, P.R. (2006). Permeability up-scaling using haar wavelets. Transp. Porous Media. 67: 395-412.

[20]. Pancaldi, V., King, P. and Christensen, K. (2009). Hierarchical coarse-graining transform, Phys. Rev. E. 79: 360-374.

[21]. Sahimi, M., Hughes, B.D., Scriven, L.D. and Davis, H.T. (1983). Real-space renormalization and selective-medium approximation to the percolation conduction problem, Phys. Rev. B. 28 (1): 307-311.

[22]. Ghoreishi, F., Tokhmechi, B., Roshandel Kahoo, A. and Ahmadi Noubari, H. (2013). A critical viewpoint on upscaling of signals in oil industry, 1st National Conference on Novelty in Computer and Information Technology, Tonekabon, Iran. 7 P.

[23]. Ghoreishi, F., Tokhmechi, B., Roshandel Kahoo, A. and Ahmadi Noubari, H. (2014). Presenting an improved approach for optimum mother wavelet selection in geosciences, Iranian Journal of Geology. 33: 79-87.

[24]. Vahedi, R., Tokhmechi, B. and Koneshloo, M. (2016). Permeability up-scaling in fractured reservoirs, using different optimized mother wavelets at each level. Journal of Mining and Environment. 7 (2): 239-250.

[25]. Gerritsen, M.G. and Durlofsky, L.J. (2005). Modeling Fluid Flow in Oil Reservoirs, Annu. Rev. Fluid Mech. 37: 211-238.

[26]. Bareiss, E.H. (1968). Sylvester's Identity and Multistep Integer-Preserving Gaussian Elimination, Math. Comput. 22: 565-578.

[27]. Gentle, J.E. (1998). Gaussian Elimination, Numerical Linear Algebra for Applications in Statistics, Berlin: Springer-Verlag. pp. 87-91.

ارائه روشی جدید برای رتبه‌بندی بلوک‌ها در فضای دو بعدی، در حالت بزرگ مقیاس‌سازی چند مقیاسیِ مبتنی بر موجک

بهزاد تخم‌چی[1*]، مینو ربیعی[2]، هاله عزیزی[2] و وامق رسولی[2]

۱- دانشکده مهندسی معدن، نفت و ژئوفیزیک، دانشگاه صنعتی شاهرود، ایران
۲- دانشکده مهندسی نفت، دانشگاه داکوتای شمالی، گرند فورکس، آمریکا

ارسال ۲۰۱۸/۱/۶، پذیرش ۲۰۱۸/۵/۱۲

* نویسنده مسئول مکاتبات: tokhmechi@ut.ac.ir

چکیده:

ساخت مدل‌های زمین‌شناسی دقیق و در واقع کوچک مقیاس، قدم اول در ارائه شبیه‌سازی قابل اطمینانی از جریان سیال در مخازن هتروژن است. اما از آنجایی که محاسبات مرتبط با مدل‌های جریان سیال بسیار زمان‌بر است، معمولاً از روش‌های بزرگ مقیاس‌سازی تک مقیاسه، به منظور کاهش زمان محاسبات، استفاده می‌شود. کاهش زمان محاسبات در مقابل از دست دادن دقت، از ویژگی‌های مدل‌های بزرگ مقیاس شده است. روش‌های متنوعی برای بزرگ مقیاس‌سازی چند مقیاسه ارائه شده‌اند، که هدف از کاربرد آن‌ها، اعمال تفاوت اندازه در بلوک‌ها است؛ به نحوی که در محدوده‌هایی از مخزن که تغییرپذیری شدیدتر است، اندازه بلوک کوچک‌تر بشود، و بالعکس. بعضی از این روش‌ها کاملاً محلی عمل می‌کنند. به عنوان مثال استفاده از روش‌های بزرگ مقیاس‌سازی مرتبط با موجک یا کرنل، در حالتی که تمایل داریم اندازه بلوک‌ها در مجاورت چاه در شبیه‌سازی‌های مرتبط با شکست هیدرولیکی کوچک‌تر بشود، توصیه شده است. در این پژوهش، یک روش جدید برای رتبه‌بندی بلوک‌ها در حالت بزرگ مقیاس‌سازی چند مقیاسی در فضای دو بعدی ارائه شده است. نتایج حاصل از اعمال روش برای یک مسئله ساده ارائه شده و معادلات جریان به منظور تشکیل ماتریس انتقال توسعه داده شده‌اند. بر اساس نتایج مدل اثبات شده که نه تنها دقت انطباق تاریخچه در حالتی که از روش ارائه شده استفاده می‌شود، افزایش می‌یابد، بلکه زمان محاسبات نیز کاهش قابل ملاحظه‌ای خواهد یافت.

کلمات کلیدی: کرنل، انطباق تاریخچه، بزرگ مقیاس سازی چند مقیاسی، زمان محاسبات.